Optics & Laser Technology 45 (2013) 190–197

Contents lists available at SciVerse ScienceDirect

Optics & Laser Technology

journal homepage: www.elsevier.com/locate/optlastec

A fast auto-focusing technique for the long focal lens TDI CCD camera in remote sensing applications

Dejiang Wang [a,c,d,*], Xu Ding [b], Tao Zhang [c], Haipeng Kuang [c]

[a] Key Laboratory of Airborne Optical Imaging and Measurement, Changchun Institute of Optics, Fine Mechanics and Physics, Chinese Academy of Sciences, Changchun 130033, China
[b] Jilin University, College of Communication Engineering, Changchun 130012, China
[c] Changchun Institute of Optics, Fine Mechanics and Physics, Chinese Academy of Science, Changchun 130033, China
[d] Graduate School of the Chinese Academy of Science, Beijing 100084, China

ARTICLE INFO

Article history:
Received 4 April 2012
Received in revised form
13 June 2012
Accepted 2 July 2012
Available online 25 July 2012

Keywords:
Time delay and integration charge coupled device (TDI CCD)
Auto focusing technique
Remote sensing application

ABSTRACT

The key issue in automatic focus adjustment for long focal lens TDI CCD camera in remote sensing applications is to achieve the optimum focus position as fast as possible. Existing auto-focusing techniques consume too much time as the mechanical focusing parts of the camera move in steps during the searching procedure. In this paper, we demonstrate a fast auto-focusing technique, which employs the internal optical elements and the TDI CCD itself to directly sense the deviations in back focal distance of the lens and restore the imaging system to a best-available focus. It is particularly advantageous for determination of the focus, due to that the relative motion between the TDI CCD and the focusing element can proceed without interruption. Moreover, the theoretical formulas describing the effect of imaging motion on the focusing precision and the effective focusing range are also developed. Finally, an experimental setup is constructed to evaluate the performance of the proposed technique. The results of the experiment show a $\pm 5\,\mu m$ precision of auto-focusing in a range of $\pm 500\,\mu m$defocus, and the searching procedure could be accomplished within 0.125 s, which leads to remarkable improvement on the real-time imaging capability for high resolution TDI CCD camera in remote sensing applications.

1. Introduction

Even in a carefully controlled environment, small thermal changes can set up thermal gradients in the optical path (glass and air) of a long focal lens imaging objective. The thermal gradients alter the wave-front by slightly changing the shape, the thickness and the refractive index of the optical elements [1,2]. Although the gradient-induced wave-front modifications are generally small, they are sufficient enough to degrade the imaging system resolution [3]. However, the significantly degraded performance could be restored to the ideal level when the optimum focus for the deformed wave-front is substituted for the nominal focus [4,5]. The laboratory calibration method is the initial focusing technique in remote sensing applications. But, the real situation encountered in the space cannot be modeled as well as possible, especially with a new design. In such cases, it is difficult to improve the focusing accuracy further. Another widely used focusing technique in remote sensing applications is the photo-electrics auto-collimation method, which has been successfully used in the long focal lens aerial camera, KA112A and KS146. As reported, the focusing precision of KA112A has approached 8 μm, and it ensures that the camera imaging resolution could reach 70lp/mm in practice. But, the focusing process occupies more than 60 s, which degrades the system real time imaging capability dramatically. With the extensive usage of CCD in the imaging system, judging whether the camera is in focus by analyzing the captured images has been studied comprehensively [6–9]. A focus measure is a function of digital images that gives a single value for each input image as the indicator of its focusing status. Usually an optical imaging system is modeled as a linear system, and thus the image on the image sensor is the convolution of the imaging target and the system's point spread function (PSF). When an aberration-free optical system is focused on its imaging target, its PSF is an ideal dot and the image is sharp; when the optical system is out of focus, its PSF is a circular spot and the image is blurred. Nevertheless, different from the imaging conditions encountered in ground, there are other sources, such as relative motion between the ground scene and the image sensor [10,11], blurring the image in the space. In such a situation, the calculated focus measures may have multiple extreme values during the searching procedure, and the local

* Corresponding author at: Key Laboratory of Airborne Optical Imaging and Measurement, Changchun Institute of Optics, Dongnanhu Road No3888, Changchun 130033, China. Tel.: +86 431 86176158; fax: +86 431 85680049.
E-mail address: wangdj04@ciomp.ac.cn (D. Wang).

0030-3992/$ - see front matter © 2012 Elsevier Ltd. All rights reserved.
http://dx.doi.org/10.1016/j.optlastec.2012.07.005

optima can cause miscalculation of the position of the captured images. These problems will, in turn, affect the focusing accuracy greatly. Moreover, these focusing techniques are mainly suitable for the area CCD camera due to that the best focus position is derived by processing the defocused images in frame.

The time delay and integration mode of the CCD provides the increased sensitivity without sacrificing the spatial resolution, and the TDI CCD is used more extensively in remote sensing applications for improving the low light level capability [12–14]. Unfortunately, there has been little research on the focusing technique for the TDI CCD camera specially. In consideration of such a situation, a high performance auto-focusing technique counteracting the residual effects of temperature shifts and thermal gradients is introduced in Section 2, whereby the optimum focus position of the lens is determined utilizing the self-imaging of the TDI CCD camera under a broad range of temperature and pressure condition. Moreover, the influence of the continuously searching scheme on the focusing performance is studied thoroughly, and the detail mathematical deviations are illustrated in Section 3. Furthermore, the proposed focusing technique has been successfully employed in a long focal lens TDI CCD camera, and the experimental results are presented, and then discussed in Section 4.

2. The auto-focusing technique evaluation

2.1. The auto-focusing techniques comparison

There exist two major focus searching methods: depth-from-focusing (DFF) and depth-from-defocusing (DFD) [15–18], and Fig. 1 illustrates their motion trajectories during the searching procedure. The DFF method uses a sequence of images taken by changing the focus setting of the imaging optics in small steps, and the object should be focused within the searching range, so the mechanical focusing parts will execute the actions of the starting, the braking and the holding repeatedly for many times. Assuming that the DFF technique requires acquiring and processing 20 images, so $20\times n$ seconds is needed at least, where n represents the time required for the focusing elements moving from one position to the adjacent position. While the DFD method uses only two images with different optical settings, and the objects need not be focused, thus the DFD method will consume $2\times n$ seconds approximately. It could be seen obviously that the DFD method is significantly superior to the DFF method in terms of the searching efficiency. However, the DFD technique suffers from the problem of the limited range of effectiveness and high noise sensitivity, thus they are in general less accurate than the DFF method, and the DFF technique is widely acknowledged as the preferred focus searching scheme in the condition where the requirement of the focusing performance is relatively higher, such as in remote sensing applications for the long focal lens camera.

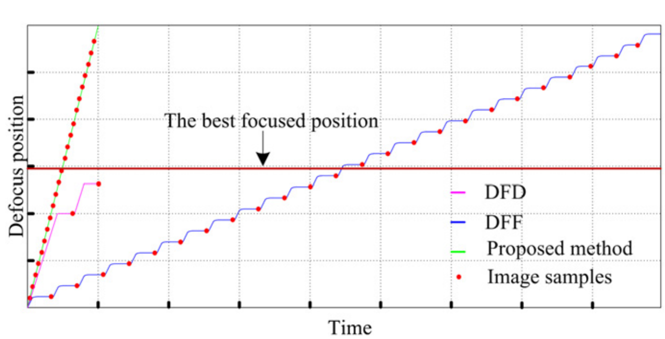

Fig. 1. Motion trajectories of the DFF, DFD and the proposed focusing techniques.

The existing DFF technique suffers from the problem that the time for approaching the best focus position is too long. It is because that the mechanical focusing parts of the camera should keep stable at the imaging instant, so the focusing mechanical elements will move in steps until the observed image of the target is in sharpest focus, thus too much time has been wasted. Therefore, it is reasonable to conclude that combining the multiple discrete actions into a continuous movement would improve the searching efficiency greatly. As Fig. 1 shows, the proposed searching technique acquires the images during continuous execution of the relative motion between the sensor and the focusing elements, which results in appreciably fast determination of the optimum focus. In the following section, the details of the technique will be presented. Aside from above presentation, noting that the relative motion between the target and the photosensitive pixel will cause image blurring, then affect the focusing accuracy more or less. Therefore, the influence of the proposed focusing scheme on the focusing performance should also be analyzed thoroughly.

2.2. The proposed auto-focusing technique

As Fig. 2 shows, the auto-focusing system consists of an independent light source with a small ronchi target, the imaging sensor itself, a precision focal plane drive mechanism, the frame grabber, the focus measure processor and the optical elements, including the scan mirror used for auto collimating. Considering that the ronchi target has high spatial frequency components along the bars alignment direction solely, and the TDI CCD could only detect high frequency components across the charge transfer direction without motion compensation, it is required that the orientation of the TDI CCD charge transfer should be perpendicular to the bar alignment orientation of the ronchi target. At the start of the auto focus, the target located at the image plane is illuminated by the independent light source. The resulting beam is collimated by the lens, and then reflected off the scan mirror which has been positioned to provide auto collimation. Finally, the return beam is imaged upon the TDI CCD.

Fig. 3 depicts the method for determining the optimum focus position. The arrival for the focusing mirror at the beginning position is performed from instantaneous position to starting position

$$z_s = z_0 - r/2 \tag{1}$$

where z_0 represents the estimated focus position according to the ambient temperature and the atmospheric pressure provided by the sensors mounted on the camera, and r represents the searching region along the Z direction.

Unlike traditional DFF method, the focusing mirror will move continuously within the total back-focus correction range at a constant velocity during the searching procedure, and the TDI

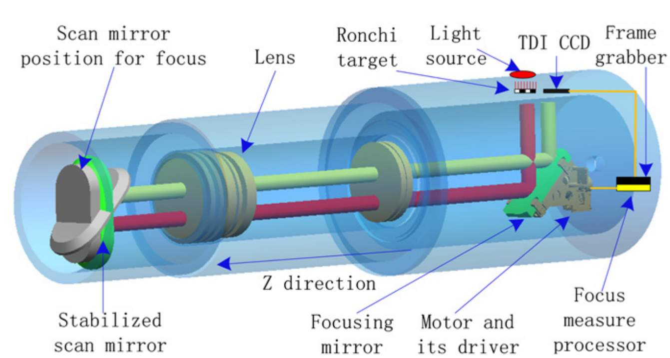

Fig. 2. Block diagram of the auto-focusing system.

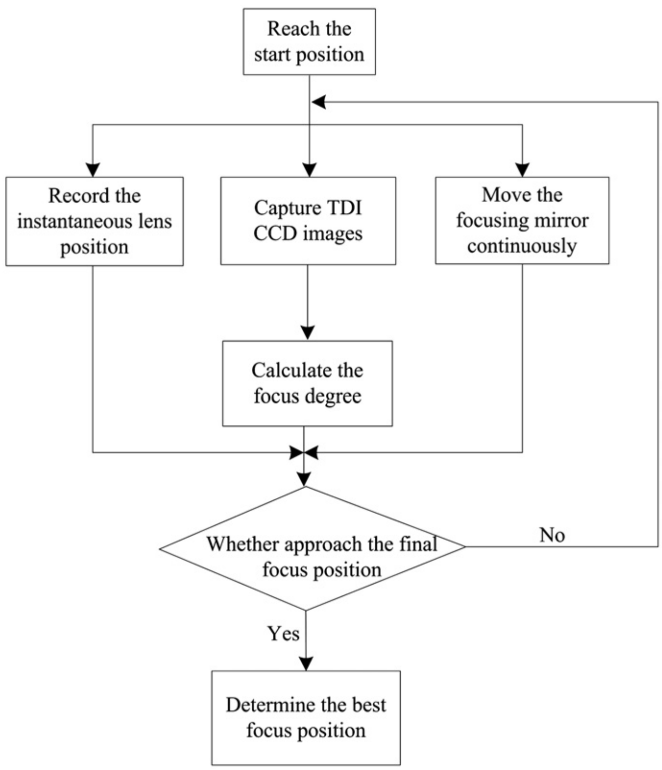

Fig. 3. Block diagram for determining the optimal focus position.

CCD will operate at the given line frequency and integration stage. Acquisitions of the images and the associated lens position are performed concurrently with motion of the focusing mirror, and the contrast degree for each line of the image is calculated in real time. Movement through the focus capture region is performed until the following final position is approached

$$z_f = z_0 + r/2 \tag{2}$$

Generally, the profile of the real focus measure is continuous based on the identified discrete value by means of a polynomial interpolation, and the interpolating $N-1$ order polynomial that proceeds through the N points using the Lagrange formula

$$p = \frac{(x-x_2)(x-x_3)\cdots(x-x_N)}{(x_1-x_2)(x-x_3)\cdots(x_1-x_N)}y_1 + \frac{(x-x_1)(x-x_3)\cdots(x-x_N)}{(x_2-x_1)(x_2-x_3)\cdots(x_2-x_N)}y_2 + \cdots + \frac{(x-x_1)(x-x_2)\cdots(x-x_{N-1})}{(x_N-x_1)(x_N-x_3)\cdots(x_N-x_{N-1})}y_N \tag{3}$$

when the value pairs of the focus measure are inserted into Eq. (3) as points, the polynomial of a continuous focus measure is obtained. The characteristic of the focus measure is that the maximum value occurs where the image contrast is highest (when the target is in the best focus position). Therefore, the best focus position for the available wave-front could be determined according to the interpolated curve. However, it should be emphasized that the focus position determined by our method is the optimal lens focus position at infinity. Considering the effect of the distance between the scene and the imaging system on the amount of defocus, the real best focus position should be further adjusted according to the geometrical optics formulations.

3. Theoretical analysis of the auto-focusing technique

3.1. The focusing performance evaluation

Fig. 4 shows a typical plot of a focus measure as a function of the lens position by means of a polynomial interpolation. We find that the expected value of the focus measure near the maximum value could be modeled by a quadratic polynomial or other models, such as cubic or Gaussian. Nevertheless, such extensions do not appear to offer significant advantages compared to the quadratic model in practical applications. For simplicity, the formulation of the solid curve shown in Fig. 4 is expressed using quadratic polynomial

$$\overline{\upsilon(p)} = ap^2 + bp + c \tag{4}$$

where $\overline{\upsilon(p)}$ represents the expected value of the focus measure with respect to the lens position p.

Let the focus measure be given at three arbitrary positions which are δapart, for example, $p_- = -\delta$, $p_0 = 0$, $p_+ = \delta$. Solving for the coefficients of Eq. (4), we obtain

$$a = \frac{\overline{\upsilon(p_+)} + \overline{\upsilon(p_-)} - 2\overline{\upsilon(p_0)}}{2\delta^2}, \quad b = \frac{\overline{\upsilon(p_+)} - \overline{\upsilon(p_-)}}{2\delta^2} \tag{5}$$

Let $\overline{p_m}$ be the expected value of the lens position where the focus measure becomes the maximum, from Eq. (5) we obtain

$$\begin{aligned}\overline{p_m} &= -\frac{b}{2a} \\ &= \frac{\delta}{2}\frac{\overline{\upsilon(p_+)} - \overline{\upsilon(p_0)}}{\overline{2\upsilon(p_0)} - \overline{\upsilon(p_+)} - \overline{\upsilon(p_-)}}\end{aligned} \tag{6}$$

It needs to be emphasized that the formulations shown in Eqs. (4)–(6) are generated by the traditional step searching method, which indicates that one focus measure corresponds to only one frame of image captured at some lens position. However, for the proposed searching scheme, the final image of the TDI CCD will be the summation of the collections at different lens position. Then for the proposed searching scheme the expected value of the focus measure at lens position p is given by

$$\begin{aligned}\overline{\upsilon'(p)} &= \sum_{n=-N/2}^{N/2} (a(p+n\sigma)^2 + b(p+n\sigma) + c) \\ &= (N+1)(ap^2 + bp + c + a\frac{N(N+2)}{12}\sigma^2)\end{aligned} \tag{7}$$

where σrepresents the displacement of the lens position between two adjacent exposure stages, and $N+1$ represents the TDI CCD integration stage.

Similar to the formulas given in Eq. (6), the position where the focus measure approaches the maximum value for the proposed

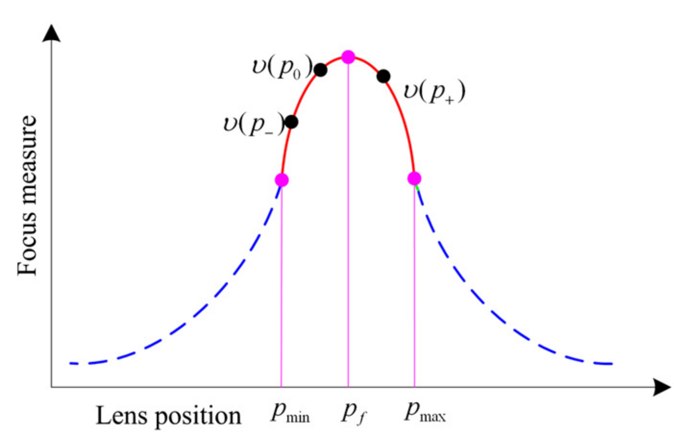

Fig. 4. Quadratic polynomial interpolation for the conventional focus measure.

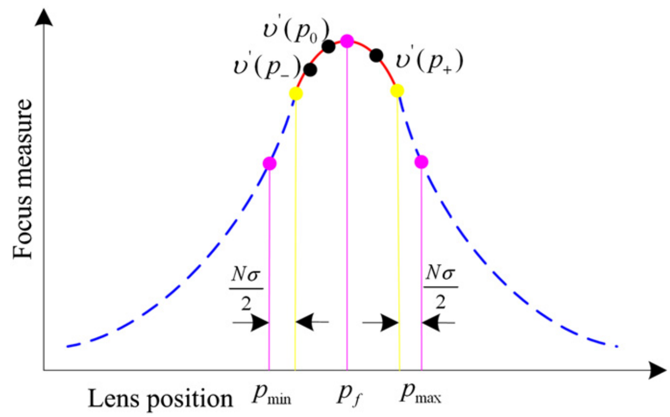

Fig. 5. Quadratic polynomial interpolation for the proposed focus measure.

searching scheme is given by

$$\overline{p'_m} = \frac{\delta}{2}\frac{\overline{\upsilon'(p_+)}-\overline{\upsilon'(p_0)}}{2\overline{\upsilon'(p_0)}-\overline{\upsilon'(p_+)}-\overline{\upsilon'(p_-)}} \tag{8}$$

Substituting Eq. (7) into Eq. (8), we obtain

$$\begin{aligned}\overline{p'_m} &= \frac{\delta}{2}\frac{(ap_+^2+bp_++c)-(ap_-^2+bp_-+c)}{2(ap_0^2+bp_0+c)-(ap_+^2+bp_++c)-(ap_-^2+bp_-+c)}\\ &= \frac{\delta}{2}\frac{\overline{\upsilon(p_+)}-\overline{\upsilon(p_0)}}{2\overline{\upsilon(p_0)}-\overline{\upsilon(p_+)}-\overline{\upsilon(p_-)}}\\ &= \overline{p_m}\end{aligned} \tag{9}$$

From Eq. (9), it could be seen that the expected value of the lens position, where the focus measure reaches its maximum value by our method, keeps unchanged when compared to the correspondence determined by the traditional searching scheme, and it also indicates that the best focus position determined by our method is just the real optimal focus position at infinity.

Compared to the expected value of the best focus lens position, we are more interested in the root mean square (RMS) value of p'_m due to that it represents the focusing performance. For this reason, the real focus measure $\upsilon'(p)$ will be expressed as the summation of the expected value $\overline{\upsilon'(p)}$ as well as the noise component $n'(p)$ [19,20]

$$\upsilon'(p) = \overline{\upsilon'(p)} + n'(p) \tag{10}$$

In this way, Eq. (8) is rewritten as

$$\begin{aligned}p'_m &= \frac{\delta}{2}\left(\frac{\upsilon'(p_+)-\upsilon'(p_-)}{2\upsilon'(p_0)-\upsilon'(p_+)-\upsilon'(p_-)}\right)\\ &= \frac{\delta}{2}\left(\frac{(\overline{\upsilon'(p_+)}+n'(p_+))-(\overline{\upsilon'(p_-)}+n'(p_-))}{2(\overline{\upsilon'(p_0)}+n'(p_0))-(\overline{\upsilon'(p_+)}+n'(p_+))-(\overline{\upsilon'(p_-)}+n'(p_-))}\right)\\ &= \frac{\delta}{2}\left(\frac{\overline{\upsilon'(p_+)}-(\overline{\upsilon'(p_-)}}{2\overline{\upsilon'(p_0)}-\overline{\upsilon'(p_+)}-\overline{\upsilon'(p_-)}}\right)\left(1+\frac{n'(p_+)-n'(p_-)}{\overline{\upsilon'(p_+)}-\overline{\upsilon'(p_-)}}\right)\\ &\quad\left(1+\frac{2n'(p_0)-n'(p_+)-n'(p_-)}{2\overline{\upsilon'(p_0)}-\overline{\upsilon'(p_+)}-\overline{\upsilon'(p_-)}}\right)\end{aligned} \tag{11}$$

Near the focused position, we have $\overline{\upsilon'(p_0)} > \overline{\upsilon'(p_+)}$ and $\overline{\upsilon'(p_0)} > \overline{\upsilon'(p_-)}$. Therefore, if the signal to noise ratio is sufficiently high, from Eq. (11) we obtain

$$\begin{aligned}p'_m &= \frac{\delta}{2}\left(\frac{\overline{\upsilon'(p_+)}-(\overline{\upsilon'(p_-)}}{2\overline{\upsilon'(p_0)}-\overline{\upsilon'(p_+)}-\overline{\upsilon'(p_-)}}\right)\left(1+\frac{n'(p_+)-n'(p_-)}{\overline{\upsilon'(p_+)}-\overline{\upsilon'(p_-)}}\right)\\ &= \overline{p'_m} + \frac{\delta}{2}\left(\frac{n'(p_+)-n'(p_-)}{2\overline{\upsilon'(p_0)}-\overline{\upsilon'(p_+)}-\overline{\upsilon'(p_-)}}\right)\end{aligned} \tag{12}$$

Then the auto focusing root mean square error is

$$\mathrm{RMS}(p'_m) = \frac{\delta}{2}\frac{\sqrt{n'(p_+)^2+n'(p_-)^2}}{2\overline{\upsilon'(p_0)}-\overline{\upsilon'(p_+)}-\overline{\upsilon'(p_-)}} \tag{13}$$

It indicates that the auto focusing root mean square error decreases with increasing signal to noise ratio, therefore, it is required that the illumination of the light source shown in Fig. 2 should be higher enough for improving the focusing accuracy.

3.2. The effective focusing range

As mentioned above, Eq. (4) is only tenable within the range of $(p_{\min},p_{\max})$. If the lens position goes beyond the threshold, the formulation of the focus measure will be indeterminate. From Eq. (7), it could be seen that the focus measure resolving from the proposed searching scheme is composed of the contributions at lens position $(p-(N\sigma/2),\ p+(N\sigma/2))$. Since the interpolated curve is higher order polynomial formulated in these regions, therefore, the focus measure within the range of $(p_{\min},p_{\min}+(N\sigma/2))$ and $(p_{\max}-(N\sigma/2),\ p_{\max})$ could not be represented using the quadratic polynomial given in Eq. (4). Then the effective range for the proposed searching scheme becomes $(p_{\min}+(N\sigma/2),\ p_{\max}-(N\sigma/2))$, which is marked by the solid line in Fig. 5.

In order to reconstruct the original signals as well as possible, it is required that three focus measure samples should be contained in the effective range at least, so it is required that

$$\left(p_{\max}-\frac{N\sigma}{2}\right)-\left(\min+\frac{N\sigma}{2}\right) > 3N\sigma \tag{14}$$

Assuming that the moving speed of the focusing mechanical element is V, the TDI CCD line frequency is f_c, then the displacement between two adjacent exposure stages is v/f_c. Thus, from Eq. (14) we obtain

$$V < \frac{(p_{\max}-p_{\min})f_c}{4N} \tag{15}$$

which indicates that the focusing element should not move too fast, otherwise the curve near the maximum focus measure value will be no longer locally smooth with respect to lens position, and it will also lead to multiple extreme values during the searching procedure.

4. Experimental results

The block diagram of the experimental devices, which are classified into two parts by function, are depicted in Fig. 6a, and the corresponding practical experimental devices are illustrated in Fig. 6b. First, an enclosed environmental testing plant is used to provide the condition which the remote sensing system encounters in the space. Second, the target beam, which is illuminated by the light source, goes through the collimator, the reflecting mirror, the tested camera lens, and then forms the image of the measured samples on the TDI CCD. For mechanical stability, the entire experimental apparatuses are mounted on top of a standard optics vibration isolation platform, which is floated to provide vibration isolation.

The proposed focusing technique, which has been well illustrated in Section 2.2, is implemented in a real TDI CCD camera, and the detail optics parameters, the detector characteristics as well as the experimental conditions are summarized in Table 1. The experiment includes two steps. First, to evaluate the proposed auto-focusing technique by the TDI CCD camera itself, and second, to test the proposed method by analyzing the captured target patterns.

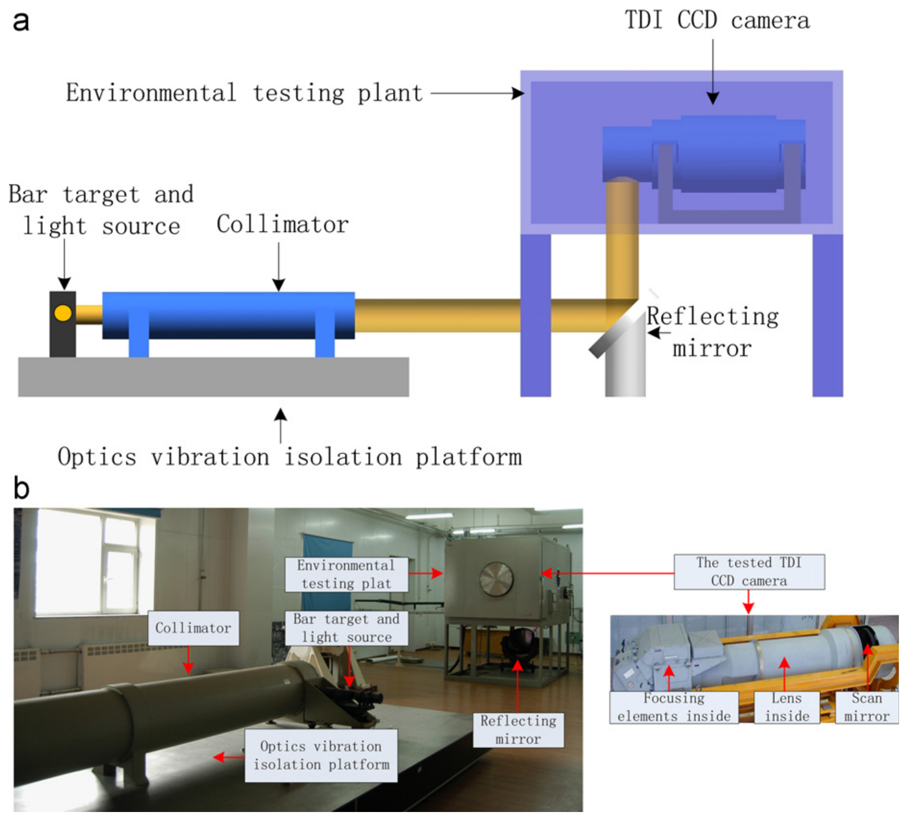

Fig. 6. (a) Block diagram of the experimental platform. (b) Practical setups of the experimental platform.

Table 1
Detail features of the testing environment.

Parameter	Value
Optics aperture diameter (mm)	300
Focal length (mm)	1800
Spectral band pass (μm)	0.4 to 0.9
Optics transmission	0.7
TDI CCD native resolution	4096
Pixel size (μm)	7
TDI stage	32
Line frequency(Hz)	250
Testing temperature (°C)	−40
Atmospheric pressure(Pa)	1200
Speed of the focusing mirror(mm/s)	1,2,4,8
Focusing correction range (mm)	1

4.1. *The searching scheme experiment*

When the focus function takes place, the focusing mirror arrives at the starting position, which has been defined in Eq. (1). Next, the mirror will move at a constant velocity, and the movement through the focus capture region is performed until a final position given in Eq. (2) is reached. Trigger signals synchronize in time with the image and the focusing mirror position acquisitions. The image capture, which is performed concurrently with motion of the focusing mirror, is accomplished by the TDI CCD, then they are transmitted to the frame grabber. A contrast calculation is implemented by the focus measure processor, and the focus measure determines the contrast value of each individual line image. In determination of the contrast, it is not necessary to employ the entire individual image. As a rule, it is sufficient to limit the contrast determination to a central sub region of the individual image. After the focus measurement, an allocation of the position values to the respective contrast values is performed. Finally, the contrast values are plotted on the ordinate as a function of the defocus lens positions, which is similar to the diagram shown in Fig. 5. From them, a determination of the suitable focus position could be made by the means described in Section 3.1.

In this experiment, the mirror moves at the speed of 1 mm/s, 2 mm/s, 4 mm/s and 8 mm/s, respectively, and Fig. 7 shows the corresponding captured target patterns. The vertical resolution of the captured image is given by

$$H = Lf_c/V \tag{16}$$

where L represents the focusing correction range, f_c represents the TDI CCD line frequency, and V represents the speed of the focusing mirror. Substituting the parameters summarized in Table 1 into Eq. (16), we obtain that the proportional factor of the vertical resolution for the four drone patterns is 1:1/2:1/4:1/8, which accords well with the images shown in Fig. 7. Since the TDI CCD line frequency is 250 Hz, so the time interval between two adjacent lines is 4 ms for all the four drone patterns, while the displacements between two adjacent lines are 4 μm, 8 um, 16 μm and 32 μm, respectively, which correspond to the speed of 1 mm/s, 2 mm/s, 4 mm/s and 8 mm/s. As we know, for producing a two dimensional image, the motion of the object should be synchronized to the TDI CCD line rate. Noting that there is no relative motion between the TDI CCD and the objective in the plane which is perpendicular to the Z axis, so the captured images only have high frequency components across the line transfer direction. However, it has no effect on the image contrast calculation, due to that we could obtain the image contrast information using the data in one dimension.

Judging whether an image is in focus from the captured samples is the most significant step in the auto-focusing procedure, since it has a great influence on the focusing performance[21,22]. For functions performing as focus measures, they

Fig. 7. The captured images at speed of (a) 1 mm/s, (b)2 mm/s w, (c) 4 mm/s, (d) 8 mm/s.

should be sensitive to high spatial frequencies in images. Wavelet is shown to be the foundation of a powerful new approach to signal processing and analysis [23,24], and it fulfils the requirements imposed on a focus measure, thus we use it as the tool for evaluating the focusing performance. The determined focus measure is expressed as

$$f = \sum_{k}^{4} \iint c_k^2(u,v)dudv \tag{17}$$

The one-dimensional wavelet transform is calculated for each line of the captured drone patterns, and Fig. 8 illustrates the calculated focus function which is obtained by focus measured defined in Eq. (17) for the four velocities. All the contrast values are normalized with the maximum value of the focus function, and each of the points in Fig. 8 stands for a contrast value of an acquired image. Similar to the aforementioned analysis, the proportional factor of the amount of sample points is 1:1/2:1/4:1/8, and the displacements between two adjacent samples are 4 μm, 8 μm, 16 μm and 32 μm, respectively. From the plurality of points, the proposed focus technique shows unimodal and monotonic behavior, which are the most important criteria for selecting the focus method. Near the best focus position, the candidate samples are used to calculate the optimum focused position according to Eq. (6). Then repeating above 100 times, the mean and standard deviations of the best focused position are computed, and the experimental results are summarized in Table 2. In order to facility comparison, the results derived from the DFF and DFD techniques which are described in Ref. [17,18] are also illustrated.

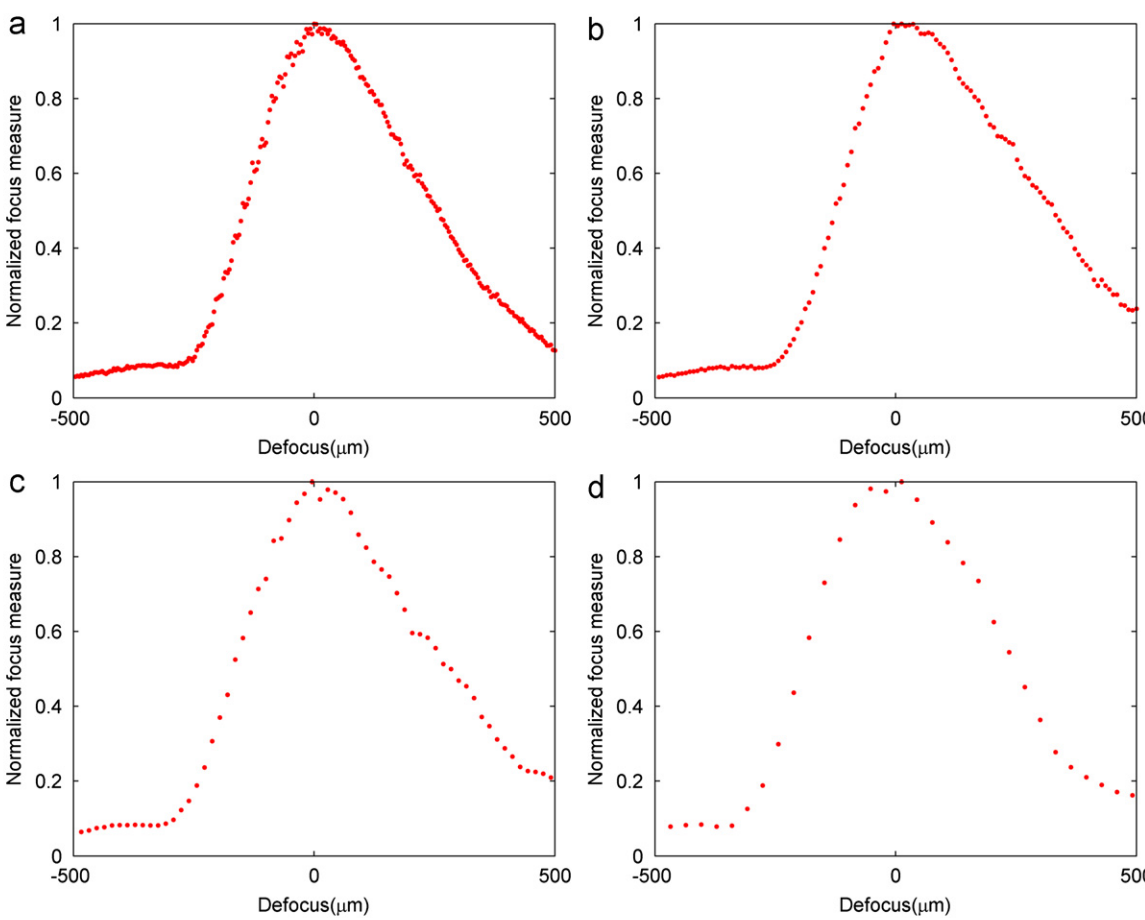

Fig. 8. The calculated focus measure at speed of (a) 1 mm/s, (b)2 mm/s, (c) 4 mm/s, (d) 8 mm/s, and the displacements between two adjacent samples are (a) 4 μm, (b) 8 μm, 16 μm, 32 μm, respectively.

Table 2
The mean and standard deviation of the focus position with different speed.

Searching scheme	Mean value of the focused position (μm)	Standard deviation of the focused position (μm)	Time requirement (s)
DFF	4.7	5.1	>10
DFD	5.6	32.4	1
S1	5.3	4.7	1
S2	-6.2	5.0	0.5
S4	7.9	8.6	0.25
S8	3.9	3.7	0.125

The proposed searching method at speed of (S1): 1 mm/s, (S2): 2 mm/s, (S4): 4 mm/s, and (S8) 8 mm/s.

Three main conclusions can be drawn from the experimental results. First, the best focus position determined by the proposed method keeps unchanged compared to the correspondence of the DFF and DFD searching methods, which accord well with the conclusion drawn in Section 3.1. It indicates that the proposed focusing technique could be used in the real imaging system. Second, the focusing accuracy for the proposed method degrades a little compared to the DFF method, but it improves a lot when compared to the results obtained from the DFD method. Noting that the negative influence on the imaging performance could be neglected due to that the position deviation is far less than half of the depth of focus, which is given by

$$\Delta = 2F^2\lambda = 36\ \mu m \tag{18}$$

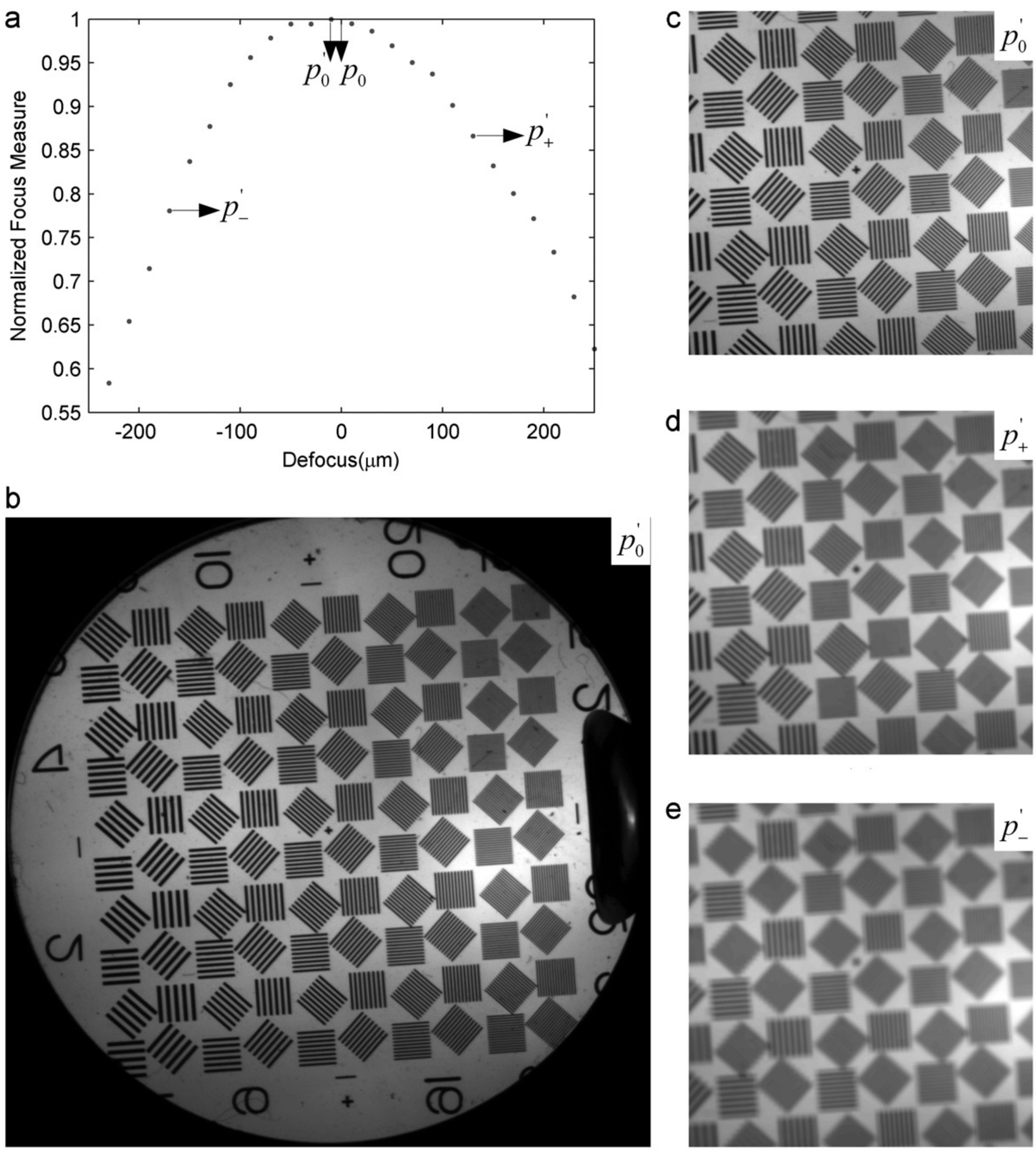

Fig. 9. The normalized focus measure with respect to the lens position (a). The lens position p_0 represents the infinity focused position determined by the proposed auto focusing technique. The lens position p_0' represents the best focus position derived from the real captured image (b), and its corresponding enlarged sectional target image is (c). The lens position p'_+ and p'_- represent two arbitrary defocus positions, and their enlarged sectional target images are (d) and (e).

Therefore, the proposed focusing technique could meet the requirement determined by the long focal lens cameras. Third, the searching efficiency could be improved by increasing the speed of the focusing mechanical element further. Nevertheless, if the time consumed during the searching process is less than some thresholds, the focusing procedure will become the image data processing limited. Furthermore, as investigated in Section 3.2, the formulated quadratic polynomial will be no longer locally smooth with respect to lens position, so it is not necessary to force the focusing mechanical element moving too fast.

4.2. The real imaging experiment

Employing the bar target, the collimator as well as the optics vibration isolation platform, the drone beam is generated which seems that the object is emitting at infinity. After reflecting, the beam will go through the camera's entrance pupil, and is incident on the TDI CCD, then forms the image of the measured samples. In this way, the focusing performance could be evaluated through the real imaging system [25,26]. Fig. 9(a) illustrates the normalized focus measure calculated from the real target patterns generated by aforementioned scheme. During searching procedure, the focusing mirror will move in steps, and the displacement between two adjacent sampling positions is 50 μm. The optimal focus position determined by real image experiment is p_0. While the best focus position determined by the proposed focusing technique is p_0'. It could be seen that the amount of the deviation from the position p_0' determined by the proposed method to the optimal focused position p_0 determined by the real imaging experiment is only 10 μm. Fig. 9(b) shows one of the candidate target pattern at the best focused position p_0'. For image interpretability convenience, we enlarged the central part of the captured target image, then it could be seen that Fig. 9(c), which is the sectional part of Fig. 9(b), demonstrates the highest contrast and exhibits the sharpest edge when compared to the correspondences shown in Fig. 9(d) and (e) captured in the defocused positions $p_-'$and p_+'. Therefore, it is reasonable to conclude that the best infinity focus position determined by the proposed auto focusing technique accords well with the real imaging results.

5. Conclusion

A fast auto focusing technique for the TDI CCD remote sensing system has been proposed. It has been successfully employed in a long focal lens camera. Different from the traditional focusing scheme, the image candidate samples used for focusing degree evaluation, are captured in the motion process, such that the focusing efficiency is improved dramatically. Moreover, the influence of the image motion on the focusing performance is analyzed thoroughly, and it shows that the optimal focused position determined by the proposed method will keep unchanged compared to the correspondence derived from the conventional step searching scheme. Furthermore, the experimental results show that the searching procedure could be accomplished as fast as 0.125 s, and the focusing accuracy could approach as higher as $\pm 5\ \mu m$ for a range of ± 0.5 mm defocusing. The proposed focusing technique demonstrates higher reliability and higher precision. Thus, it could meet the requirement of various accurate focus measurement systems.

References

[1] Iyenqar M, Lange D. The goodrich 3th generation DB-110 system: operational on tactical and unmanned aircraft. Proceedings of SPIE 2006;6209:1–12.
[2] Rao LZ, Pu JX, Chen ZY, Yei P. Focus shaping of cylindrically polarized vortex beams by a high numerical-aperture lens. Optics & Laser Technology 2009;41:241–6.
[3] Xie J, You LD, Huang SH, Duan ZC, Chen GQ. Real-time focus control in broad flat field laser material processing. Optics & Laser Technology 2008;40:330–6.
[4] M Hamborg, Autofocus method for a microscope and system for adjusting the focus for a microscope, U.S. Patent (2006) 7,027,221 B2.
[5] Wan DP, Liang XC, Meng FM, Hu DJ, Wang YM, Chen BK, Shao YM. Automatic compensation of laser beam focusing parameters for flying optics. Optics & Laser Technology 2009;41:499–503.
[6] Choi KS, Lee JS, Ko SJ. New autofocusing technique using the frequency selective weighted median filter for video cameras. IEEE Transactions on Consumer Electronics 1999;45:820–7.
[7] Zhang Y, Zhang Y, Wen C. A new focus measure method using moments. Image and Vision Computing 2000;18:959–65.
[8] Kautsky J, Flusser J, Zitova B, Simberova S. A new wavelet-based measure of image focus. Pattern Recognition Letters 2002;23:1785–94.
[9] Tian YB. Autofocus using image phase congruency. Optics Express 2011;19: 261–70.
[10] Wang DJ, Zhang T, Kuang HP. Clocking smearing analysis and reduction for multi phase TDI CCD in remote sensing system. Optics Express 2011;19: 4868–80.
[11] Wu JG, Zheng ZZ, Feng HJ, Xu ZH, Li Q, Chen YT. Restoration of TDI camera images with motion distortion and blur. Optics & Laser Technology 2010;42: 1198–203.
[12] Wang DJ, Zhang T. Noise analysis and measurement of time delay and integration charge coupled device. Chinese Physics B 2011;20:1–6.
[13] Holst GC. Electro-optical imaging system performance. SPIE Press; 2008.
[14] Chen L, Zhang X, Lin J, Sha D. Signal-to-noise ratio evaluation of a CCD camera. Optics & Laser Technology 2009;41:574–9.
[15] Aslantas V, Pham DT. Depth from automatic defocusing. Optics Express 2007;15:1011–23.
[16] Widjanarko T, Hardie RC. A post-processing technique for extending depth of focus in conventional optical microscopy. Optics & Laser Technology 2002;34:299–305.
[17] Subbarao M, Surya G. Depth from defocus: a spatial domain approach. International Journal of Computer Vision 1994;13:271–94.
[18] Subbarao M, Tyan J K. Selecting the optimal focus measure for autofocusing and depth-from-focus. IEEE Transactions on Pattern Analysis and Machine Intelligence 1998;20:864–70.
[19] Holst GC. CMOS/CCD sensor and camera systems. SPIE Press; 2007.
[20] Janesick JR. Scientific charge-coupled devices. SPIE Press; 2001.
[21] Tian YB, Shieh K, Wildsoet CF. Performance of focus measures in the presence of nondefocus aberrations. Journal of the Optical Society of America A 2007;24:165–73.
[22] Sun Y, Nelson BJ. Autofocusing in computer microscopy: selecting the optimal focus algorithm. Microscopy Research and Technique 2004;65: 139–49.
[23] Wang Q, Chen L, Zhou JY, Lin QH. Modified wavelet based morphological correlation for rotation-invariant recognition. Optics & Laser Technology 2011;43:1504–12.
[24] Bhagatji A, Nishchal NK, Gupta AK, Tyagi BP. Wavelet-modified fringe-adjusted joint transform correlator. Optics & Laser Technology 2008;40: 99–112.
[25] Silveira PX, Narayanswamy R. Signal-to-noise analysis of task-based imaging systems with defocus. Applied Optics 2006;45:2924–34.
[26] Thurman ST, Fienup JR. Analysis of the general image quality equation. Proceedings of SPIE 2008;6978 69780F-1～69780F-13.